Catena 215 (2022) 106305

Contents lists available at ScienceDirect

Catena

journal homepage: www.elsevier.com/locate/catena

An update of the spatial and temporal variability of rainfall erosivity (R-factor) for the main agricultural production zones of Austria

Lisbeth L. Johannsen [a,*], Elmar M. Schmaltz [a], Olivia Mitrovits [a], Andreas Klik [b], Wolfgang Smoliner [b], Shengping Wang [c], Peter Strauss [a]

[a] Federal Agency for Water Management, Institute for Land and Water Management Research, Petzenkirchen, Austria
[b] University of Natural Resources and Life Sciences (BOKU), Institute for Soil Physics and Rural Water Management, Vienna, Austria
[c] College of Hydraulic and Hydro-Power Engineering, North China Electric Power University, Beijing, PR China

ARTICLE INFO

Keywords:
Rainfall erosivity
R-factor
Spatiotemporal variability
Erosion index
Erosivity density
Austria

ABSTRACT

Rainfall erosivity is one of the key parameters influencing the degree of soil erosion. Due to the high spatio-temporal variability of rainfall erosivity and the influence of a changing climate it is crucial to use spatially well-distributed and temporally current rainfall data. Rainfall erosivity in Austria has been estimated by previous studies with varying rainfall data amounts. This study aimed to create an updated R-factor map for Austria and its main agricultural production zones based on a larger number of rainfall stations and a recent time series. As well as, compare R-factors from previous studies to identify differences in erosivity estimation. Rainfall data from 171 stations throughout Austria were gap-filled and corrected to improve data quality. Rainfall erosivity was calculated for 1995–2015 for the vegetation period and annually and used to establish two linear regressions describing rainfall erosivity as a function of mean rainfall amount. The regressions were applied to the 1 km^2 daily rainfall grids from the SPARTACUS dataset to create the spatially distributed rainfall erosivity maps. Differences in the temporal and spatial distribution of rainfall erosivity, erosion index and erosivity density between the main agricultural production zones showed areas at risk of soil erosion and timing of vulnerability. The highest rainfall erosivities were found in the agriculturally important eastern regions of Austria during the summer months. Compared to previous studies, considerable differences in local R-factor estimation were found. The significantly larger number of rainfall stations and an updated time series increased the representativeness of rainfall erosivity estimation in Austria, which can contribute to a more precise soil erosion risk assessment.

1. Introduction

Water-induced soil erosion poses a significant threat to agricultural production by removing and degrading fertile soils, as soil mechanisms like filtration, nutrient cycling, water retention and the composition of organic soil are affected by erosion. Concurrently, erosion causes multiple adverse off-site effects for humans and the environment (Horrigan et al., 2002) and poses a major threat to sustainable use of soil within Europe (Boardman and Poesen, 2006; Panagos et al., 2015b).

Because soil erosion is a multifactorial process, a common way to quantify soil loss is via models. The most frequently used model application is the Universal Soil Loss Equation (USLE) (Wischmeier and Smith, 1978) and its updated versions (Renard et al., 1997; USDA-ARS, 2013). This approach uses several determining factors of erosion to obtain long-term mean annual erosion rates. The rainfall erosivity factor (R-factor) of this model describes the influences of rainfall on soil erosion risk. Rainfall erosivity is also part of the so-called management factor (C-Factor) to account for the effect of erosivity on different crop stages during the year (Renard et al., 1997).

The effects of climate change on rainfall erosivity and the increased risk this change may bear on soil erosion processes are of concern. Studies suggest that the erosivity of rainfall has increased during the last decades as the frequency of extreme rainfall events increase (Diodato et al., 2017; Fiener et al., 2013; Klik and Konecny, 2012). Increases in climatic variability, including intensive rainfall events, also have an agitating effect on soil and intensify erosive processes (Burt et al., 2016). Predictions of erosive rainfall in 2050 also suggest changes in Austrian R-factors of <-20 to >50 N h^{-1}, with the highest increases in the Alpine

* Corresponding author at: Institute for Land and Water Management Research, Pollnbergstraße 1, 3252 Petzenkirchen, Austria.
E-mail addresses: lisbeth.johannsen@baw.at (L.L. Johannsen), elmar.schmaltz@baw.at (E.M. Schmaltz), andreas.klik@boku.ac.at (A. Klik), wolfgang.smoliner@students.boku.ac.at (W. Smoliner), peter.strauss@baw.at (P. Strauss).

https://doi.org/10.1016/j.catena.2022.106305
Received 9 November 2021; Received in revised form 24 March 2022; Accepted 11 April 2022

Table 1
Characteristics of the eight main agricultural production zones (MAPZ) of Austria and the rainfall stations within them, including the mean vegetation period rainfall P_{VP} (mm) and the mean annual rainfall P_A (mm).

MAPZ	Acronym	Area (km^2)	No. of stations	Arable land (ha)	P_{VP}	P_A
Alpenostrand	AOR	10,971	15	64,667	704	999
Alpenvorland	AVL	8,588	29	323,061	726	1,071
Hochalpen	HA	29,742	35	15,076	805	967
Kärntner Becken	KB	2,497	5	41,016	618	806
Nö. Flach- und Hügelland	NFH	10,185	21	520,551	437	550
Sö. Flach- und Hügelland	SFH	5,023	3	141,696	572	613
Voralpen	VA	9,251	39	12,339	906	1,239
Wald- und Mühlviertel	WMV	7,547	24	197,422	561	638
Austria		83,804	171	1,315,832	717	937

region and the North-eastern part of the country (Panagos et al., 2017). Therefore, continuous updates on factors controlling erosive processes are needed to ensure proper agricultural management and preventative actions for risk areas.

This has also led to the ongoing work on updating R-factor estimation in several European countries in recent years. Several methodologies have been used to find the best predictors of R-factor across different temporal and spatial resolutions (Angulo-Martínez et al., 2009; Auerswald et al., 2019; Hanel et al., 2016; Lukić et al., 2019; Meusburger et al., 2012; Schmidt et al., 2016) and elucidate whether any trends in erosivity are noticeable (Bezak et al., 2020; Petek et al., 2018).

To make the erosivity estimations reliable it is paramount to have good quality rainfall data with high spatial and temporal resolution. A time series of at least 22 years has been recommended to calculate the R-factor (Verstraeten et al., 2006; Wischmeier and Smith, 1978), although 15–20 years has also been shown to be sufficient provided a high enough number of rainfall stations (Hanel et al., 2016). Benavidez et al. (2018) highlighted the importance of applying regionally derived R-factor equations and comparing results to those from previously obtained R-factors in the same study area.

Previous erosivity studies for the territory of Austria were based on varying degrees of available data to calculate R-factors. Strauss et al. (1995) calculated an R-factor range of 47 to 138 N h^{-1} yr^{-1} from 15 rainfall stations from 1961 to 1990, while Klik and Konecny (2012) estimated R-factors between 27 and 170 N h^{-1} yr^{-1} in the north-eastern regions of Upper and Lower Austria based on 51 stations with varying time series up until 2009. As part of a more extensive European study, Panagos et al. (2015a) calculated an annual R-factor range of 35 to 435 N h^{-1} yr^{-1} for Austria based on data between 1995 and 2010 from 31 stations.

The estimation of rainfall erosivity in Austria from the previous studies is based on variable spatial and temporal data. The use of different kinetic energy-intensity (KE-I) relationships can highly affect the erosivity estimation (Nearing et al., 2017; van Dijk et al., 2002). The quality of datasets has partially not been corrected for additional factors such as discrimination between rainfall and snowfall (Auerswald et al., 2015). This reduces the comparability between studies and their representativeness for the whole of Austria. Thus, we see a need for a comprehensive investigation into the rainfall erosivity estimation for Austria and to update the R-factors based on recent, high-resolution data that can produce a reliable R-factor map for Austria.

This study aims to identify the spatial and seasonal distribution of rainfall erosivity and create an updated spatially distributed R-factor map for Austria to aid region-specific management practices in the main agricultural production zones of Austria. Furthermore, a comparison of R-factors from previous studies will identify differences in erosivity estimation and enable the discussion of methodologies.

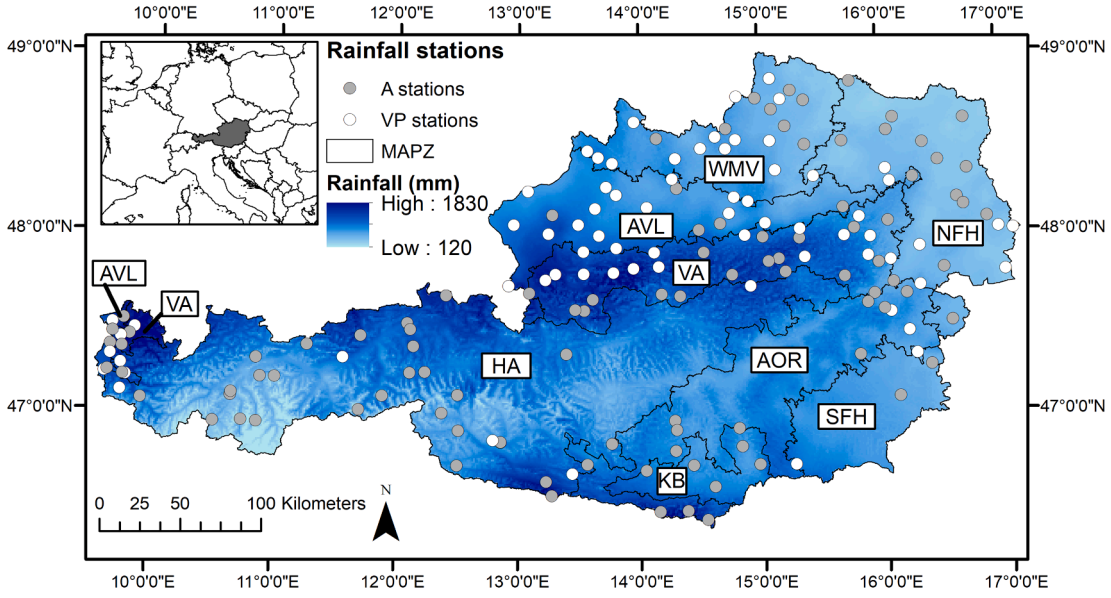

Fig. 1. Locations of all rainfall stations used for the vegetation period (VP) and the whole year (A) within each MAPZ. The base layer shows the SPARTACUS rainfall distribution (without snow) across Austria.

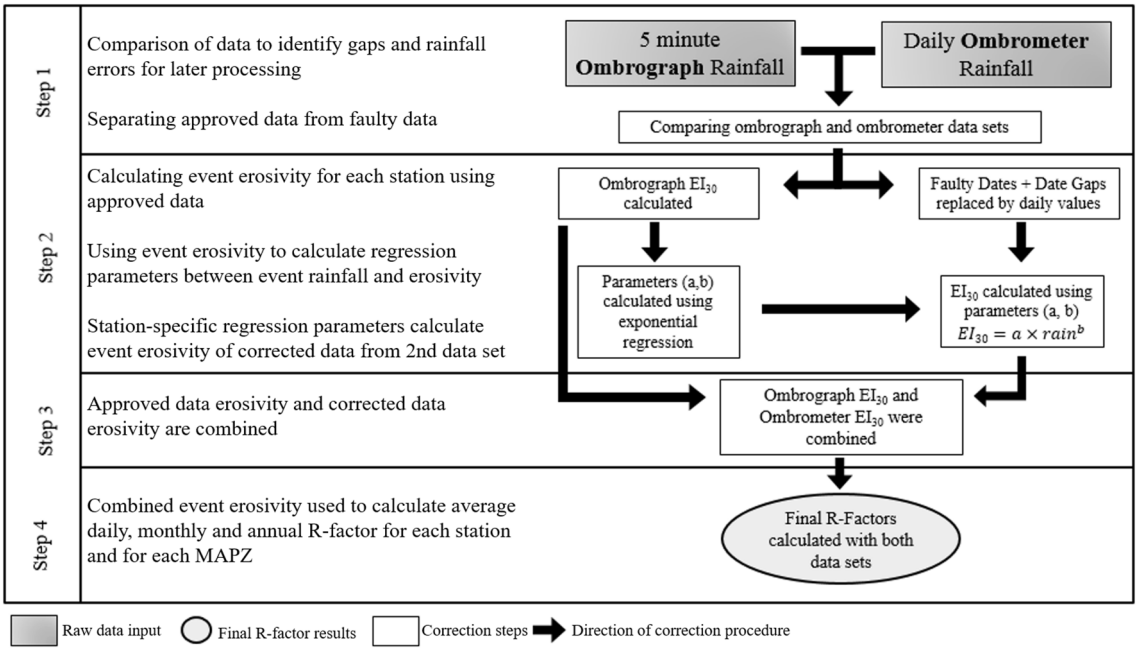

Fig. 2. Overview of the process to correct the rainfall station data used to calculate R-factors.

2. Material and methods

2.1. Study area and data

The topography of Austria varies from mountain ranges in the West, to flatlands in the East, with a wide range of elevations, climates, soil types, vegetation covers, and agricultural management practices. To account for the different landscapes and the heterogeneous agricultural crop and management systems, Austria has been classified into eight main agricultural production zones (MAPZ) based on soil characteristics, climate, terrain, agricultural production and land use (Wagner, 1990a, 1990b). Table 1 provides basic information about each MAPZ and the rainfall stations within them.

The Austrian Hydrological Survey provided rainfall (P) data from 1995 to 2015 from 171 stations to be processed for the study. The 171 stations were made up of 101 stations which could calculate an annually representative (A) temperature corrected R-factor (R) based on a 0 °C snow threshold, and the remaining 70 stations, which could be used to calculate the R-factor during the vegetation period (VP) from the 1st of April to 31st of October. The spatial distribution of all stations involved in the R-factor calculations can be seen in Fig. 1.

Each station consists of ombrographs, set at 5 min recording intervals, ranging from 18 to 21 years during 1995 to 2015. However, the data was affected by various types of errors, resulting in data gaps and incorrect recordings. To mitigate these errors and to improve the data validity, a second set of data was introduced, drawn from daily rainfall ombrometer gauges from the same stations to compare and replace defects and fill data gaps. In addition, for A stations, daily temperature data were used to distinguish snowfall from rainfall.

Austrian agricultural production is centred along the Northeast, where the highest station density is located (Fig. 1). For the agriculturally important zones AOR and SFH, station density is considerably low due to low data availability for the region. Areas in the centre of the country (found primarily in the HA zone) have the lowest density of stations. However, the topography of this region is primarily mountainous and with few cropland areas. The lack of stations was therefore not considered a drawback to the study, as the USLE approach is mainly used for cropland areas.

2.2. Rainfall erosivity (R- Factor)

Renard et al. (1997) defined an erosive rainfall event as $\geq$ 12.7 mm of rainfall, where the start and end of the event are classified by rainfall exceeding and falling below a total of 1.27 mm in 6 h. However, for this study, the European adaptation of $\geq$ 10 mm total rainfall was applied for defining an erosive event (Schwertmann et al., 1987).

To calculate the event erosivity, EI_{30} (N h^{-1}), the standard definition of the USLE was used (Wischmeier and Smith, 1978).

$$EI_{30} = \left(\sum_{r=1}^{k} e_r v_r\right) I_{30} \quad (1)$$

where e_r is the kinetic energy (kJ m^{-2} mm^{-1}), v_r is the rainfall volume (mm) in period r, and I_{30} is the maximum rainfall intensity (mm h^{-1}) within 30 min of the event.

The kinetic energy was calculated after van Dijk et al. (2002):

$$e_r = 28.3[1 - 0.52exp(-0.042 i_r)] \quad (2)$$

where i_r is rainfall intensity (mm h^{-1}) within the period r.

The kinetic energy-intensity equation by van Dijk et al. (2002) was chosen as this equation was developed as a universally predictive equation based on data from the scientific literature. When using their kinetic energy equation compared to other studies, van Dijk et al. (2002) found it to have the lowest relative difference of 0.3% between measured and predicted results.

Finally, the annual R-factor was calculated based on the sum of all annual erosive events (Wischmeier and Smith, 1978), onto which the average annual R-factor (N h^{-1} yr^{-1}) was calculated as a mean for the whole time series:

$$R = \frac{1}{n}\sum_{j=1}^{n}\sum_{k=1}^{m_j}(EI_{30})_k \quad (3)$$

where n is the number of years in the time series, m_j is the number of erosive events within a year j and EI_{30} is the rainfall erosivity of event k.

We use the unit N h^{-1} yr^{-1} for the R-factor, a common European unit (Fischer et al., 2018). A conversion to the typically also used MJ mm ha^{-1} h^{-1} yr^{-1} can be achieved by multiplying the values in N h^{-1} yr^{-1} by a factor of 10.

The erosivity density (ED) expresses the erosivity content per unit rainfall and can contribute to the assessment of areas at risk of soil erosion. Areas with a high ED may be subject to high erosivity through high-intensity rainfall and thus at risk of erosion. The monthly erosivity density, ED (N h^{-1} yr^{-1} mm^{-1}), which is the ratio between the mean monthly R-factor and the mean monthly rainfall amount of erosive rainfall, was calculated for all rainfall measurement stations:

$$ED = \frac{R}{P} \quad (4)$$

ED was also calculated for each station during the vegetation period as long-term mean R divided by long-term mean rainfall to analyse the spatial variation in ED.

In addition to the spatial distribution of the R-factor, the distribution of erosive rainfall throughout the year is essential due to the interaction of rainfall erosivity with other factors such as crop cover and management in determining soil erosion risk. Therefore, the seasonal distribution of erosive rainfall is a part of the C-factor application in the USLE soil loss estimation and is referred to as the erosion index (Wischmeier and Smith, 1978). With the intent to improve existing approaches based on a single seasonal distribution curve for the whole of Austria, daily R-factor values for all stations were calculated and aggregated into a mean seasonal R-factor distribution for each of the eight MAPZs. Similar to the study by Auerswald et al. (2019), a 30-day centred mean was applied to avoid excess scattering while maintaining the trend accuracy.

2.3. Data correction process

To improve the data quality and eliminate errors and gaps, a data correction process, as displayed in Fig. 2, was conducted by comparing ombrograph and ombrometer readings. Due to the lower error susceptibility, we considered ombrometer data as a control for this study. Thus, ombrograph data, that exceeded the daily ombrometer rainfall by ≥10 mm, were removed for further treatment. The remaining ombrograph readings were used to calculate the rainfall event erosivity (EI_{30}) and the parameters for each station. By combining the parameters with the daily ombrometer data, replacement erosivity values for the data gaps and faulty data could then be calculated and were introduced into the final R-factor valuation.

Based on the remaining ombrograph data, station-specific parameters were calculated by power-law equation, defining the relationship between event rainfall and event erosivity per station. This method is common when only daily rainfall data are available (Kinnell, 2010; Sanchez-Moreno et al., 2014; Xie et al., 2016). To ensure erosivity was only calculated for erosive events, the threshold of ≥10 mm daily rainfall was used on the ombrometer replacement data. To improve the R^2 for the replacement step, on erosive days where the next day rainfall exceeded 5 mm rainfall, the respective rainfall was added to the initial day. This improved the overall R^2 for all stations from 0.24 to 0.40, and the new (station-specific) parameters a and b (Eq. (5)) were used to calculate new erosivity values for the replacement data.

$$EI_{30} = aP^b \quad (5)$$

All stations involved in the correction process were adapted for the vegetation period R-factor (R_{VP}). To calculate an annual R-factor (R_A), stations containing temperature data could compensate for a snowfall discrepancy based on a temperature threshold of 0 °C (Leek and Olsen, 2006). A final R-factor was calculated for each station by combining the approved and treated data. The R-factors thus consisted of an average of 89% ombrograph data and 11% ombrometer data – comprising of 3% error replacements and 8% gap fillers (Table A1). The correction process resulted in an increase in total accumulated rainfall amount from all stations of 2054 mm (2%) for P_{VP} and 4194 mm (5%) for P_A. Ultimately, the correction process compensating for gaps and errors produced an overall increase of the R-factor of 8% for R_{VP} stations and 9% for R_A stations, which corresponds to an increase in the mean R-factor of 9.3 N h^{-1} yr^{-1} for R_{VP} and 10.9 N h^{-1} yr^{-1} for R_A stations.

Table 2
The number of stations used for VP (No_{VP}) and A periods (No_A) in each MAPZ and the whole of Austria, mean R_{VP}- and R_A-factors (N h^{-1} yr^{-1}) calculated based on rainfall station data and their standard deviation, and erosivity density for VP (ED_{VP}) and A (ED_A) periods (N h^{-1} yr^{-1} mm^{-1}) and their standard deviation.

MAPZ	No_{VP} (No_A)	R_{VP}	R_A	ED_{VP}	ED_A
AOR	15 (11)	142 (±55)	168 (±100)	0.25 (±0.07)	0.23 (±0.12)
AVL	29 (11)	119 (±37)	142 (±75)	0.24 (±0.03)	0.20 (±0.10)
HA	35 (30)	111 (±56)	113 (±71)	0.18 (±0.03)	0.16 (±0.06)
KB	5 (5)	116 (±16)	124 (±13)	0.24 (±0.04)	0.21 (±0.03)
NFH	21 (14)	71 (±17)	73 (±36)	0.27 (±0.03)	0.25 (±0.12)
SFH	3 (2)	125 (±26)	111 (±52)	0.30 (±0.03)	0.28 (±0.13)
VA	39 (20)	167 (±60)	186 (±108)	0.24 (±0.03)	0.21 (±0.10)
WMV	24 (8)	92 (±18)	96 (±46)	0.27 (±0.03)	0.27 (±0.13)
Austria	171 (101)	121 (±55)	130 (±69)	0.24 (±0.05)	0.21 (±0.05)

2.4. Mapping of rainfall erosivity

In order to spatially extend the point data of R-factor values, 1 km^2 cell grids of daily rainfall and temperature NetCDF data files were obtained from the Austrian SPARTACUS project (Hiebl and Frei, 2018, 2016). The rainfall data consists of krigged and cross-validated monthly precipitation readings combined with daily anomalous recordings to create daily 1 km^2 raster grids of continuous data since 1961 based on 523 rainfall stations. The same process was used for temperature data to create continuous 1 km^2 raster grids, albeit from 428 stations. We refer

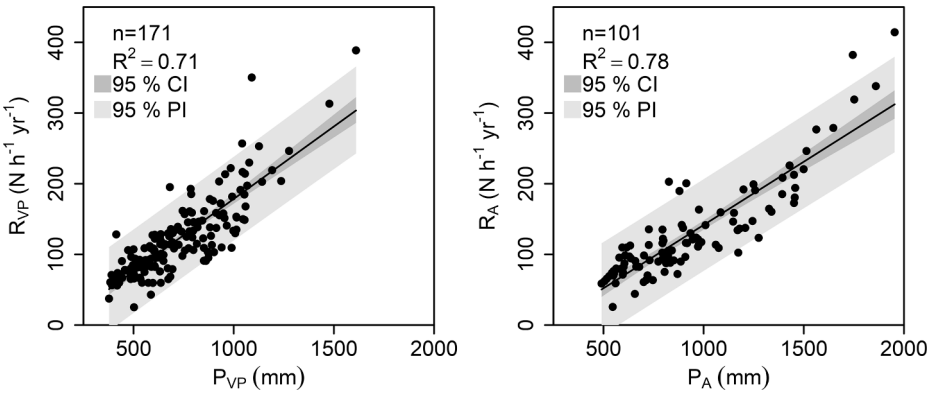

Fig. 3. Relationships between mean rainfall and R-factor for the VP (left) and A (right) stations, including the 95% confidence interval (CI) and 95% prediction interval (PI) of the linear regression.

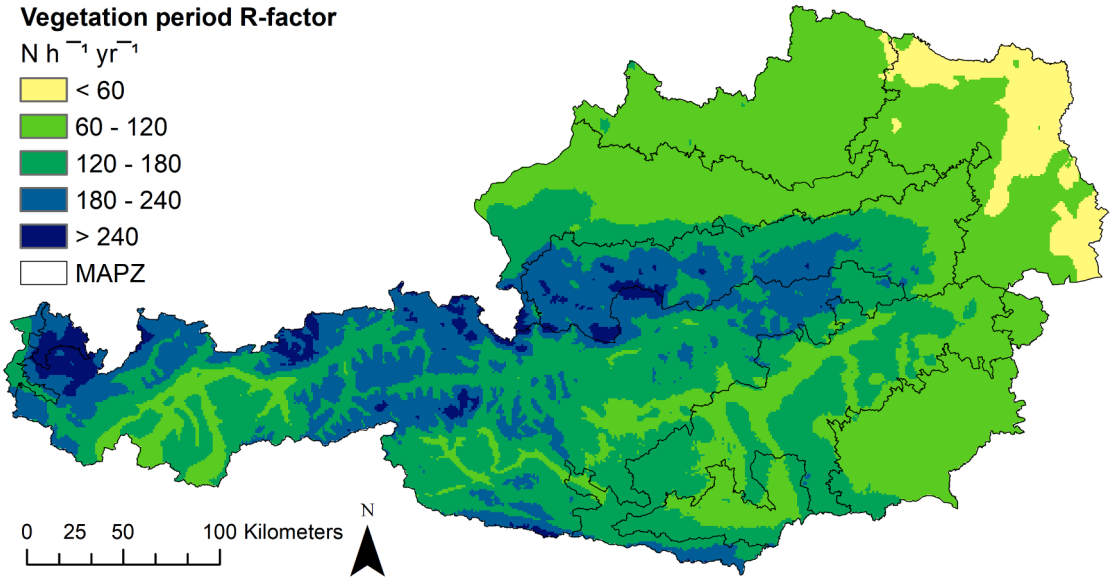

Fig. 4. Map of R_{VP}-factors (N h^{-1} yr^{-1}) based on 1 km grid cell for Austria and each MAPZ.

to Hiebl and Frei (2018, 2016) for further information on the datasets.

The R-factor maps for Austria and the individual MAPZs were generated in the following steps:

1. Overlap of the rainfall and temperature grids and removal of rainfall grid cell values observed on days below the snow temperature threshold of 0 °C.
2. Generation of mean annual and mean vegetation period rainfall grids for Austria based on the SPARTACUS daily grid data from 1995 to 2015.
3. Spatial R-factor calculation by inserting the mean rainfall of each grid cell of the VP and A grids in the R_{VP} and R_A linear regressions, respectively.

2.5. Comparison of studies and validation of rainfall erosivity

To explore changes in past to present erosivity results, a comparison to previous Austrian erosivity studies was made. The R-factor regressions from Strauss et al. (1995) (annual and summer) and Klik and Konecny (2012) were used on the same SPARTACUS data as our regressions to create a spatial R-factor map. The R-factor map of Panagos et al. (2015a) was clipped to Austria, and the cell size changed to 1 km^2 to be comparable to our R_A map. Our R-factor maps were subtracted from the R-factor maps of the previous studies, and the range, mean and standard deviation of differences calculated. All map calculations were done in ESRI ArcGIS (version 10.8.1).

Further, a comparison of the R-factor maps and the R-factors from each rainfall station was carried out to validate the results. This was done by finding the R-factor of the grid cell at the location of each rainfall station for each R-factor map and comparing the R-factor values based on three statistical indices. The statistical indices were mean absolute error (MAE), root mean squared error (RMSE) and Wilmott's agreement index (WI), following those used in previous studies (Angulo-Martínez et al., 2009; Hanel et al., 2016).

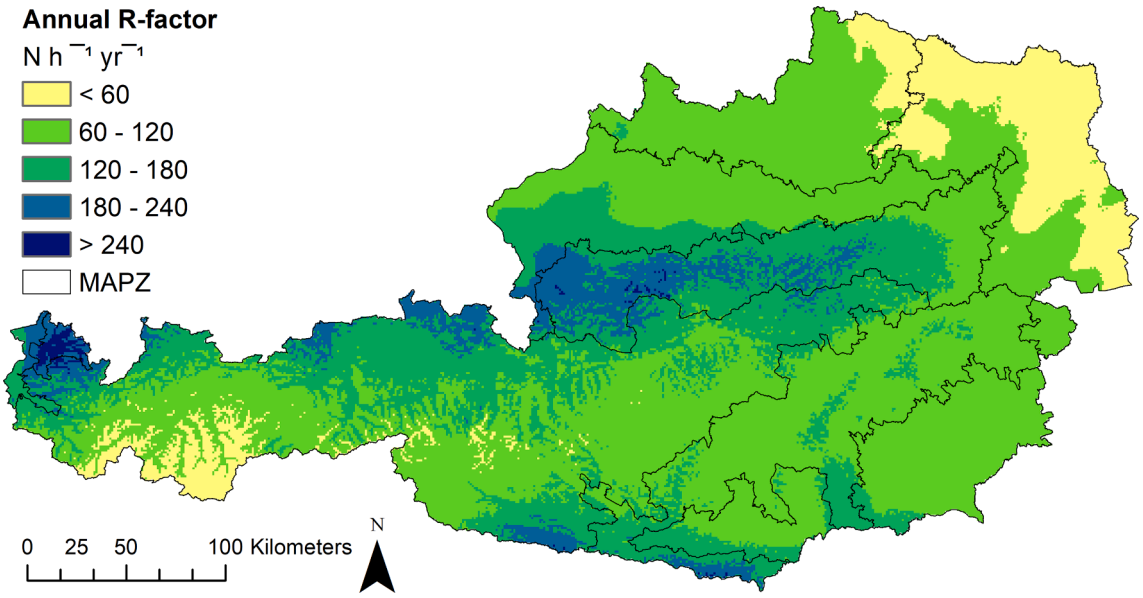

Fig. 5. Map of R_A-factors (N h^{-1} yr^{-1}) based on 1 km grid cell for Austria and each MAPZ.

Table 3
Mean R-factors R_{VP} and R_A (±standard deviation) in N h^{-1} yr^{-1} and mean rainfall P_{VP} and P_A (±standard deviation) in mm for each MAPZ and Austria based on the spatially distributed map for R_{VP} and R_A for the VP and A periods.

MAPZ	R_{VP}	R_A	P_{VP}	P_A
AOR	130 (±25)	112 (±25)	764 (±120)	835 (±140)
AVL	116 (±32)	119 (±32)	697 (±156)	872 (±179)
HA	168 (±39)	116 (±40)	947 (±189)	858 (±222)
KB	124 (±17)	115 (±18)	736 (±85)	850 (±100)
NFH	64 (±9)	59 (±9)	443 (±42)	539 (±48)
SFH	101 (±14)	93 (±14)	622 (±66)	729 (±78)
VA	172 (±48)	159 (±43)	969 (±232)	1095 (±240)
WMV	90 (±15)	81 (±18)	568 (±73)	661 (±99)
Austria	133 (±49)	109 (±41)	779 (±241)	818 (±230)

3. Results and discussion

3.1. Rainfall erosivity in Austria

Based on the borders of the eight MAPZs, the final R-factors were calculated for VP and A defined data for all rainfall stations (Table 2).

The mean R-factors calculated from station rainfall data were 121 N h^{-1} yr^{-1} and 130 N h^{-1} yr^{-1}, ranging between 25 and 389 N h^{-1} yr^{-1} and 26 to 414 N h^{-1} yr^{-1} for VP and A stations, respectively. Of the MAPZ, Voralpen (VA) measured the highest R_{VP} and R_A with 167 and 186 N h^{-1} yr^{-1}, respectively. Comparatively, the lowest R_{VP} and R_A were found in NFH and WMV, which also experienced low precipitation rates (Hiebl and Frei, 2018). The R-factors of individual stations can be found in Table A1 in the appendix of this paper.

Comparing our calculated R-factors for the stations with those found in the countries surrounding Austria, similar values were found in

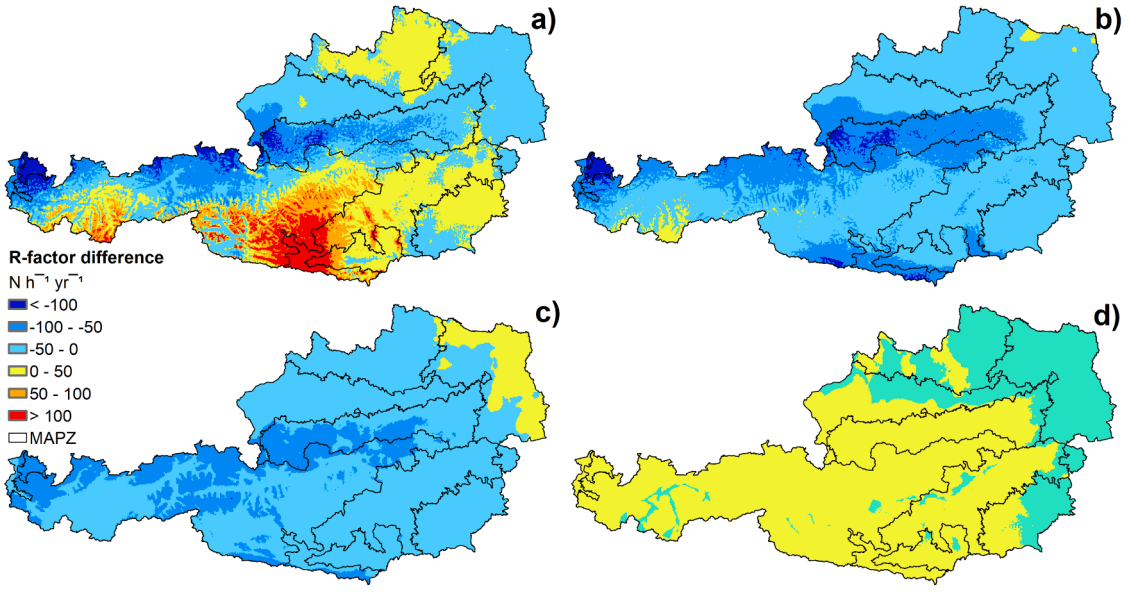

Fig. 6. R-factor difference (N h^{-1} yr^{-1}) between the R_A-factor map and the map of **a)** Panagos et al. (2015a), **b)** Strauss et al. (1995) annual regression, and between the R_{VP}-factor map and that of **c)** Strauss et al. (1995) summer regression, **d)** Klik and Konecny (2012).

Switzerland. Meusburger et al. (2012) found the R-factor based on station data to range between 12 and 561 N h^{-1} yr^{-1} with a mean of 133 N h^{-1} yr^{-1}. In Germany, the R-factors for 115 rain gauges were found to have a mean of 90 N h^{-1} yr^{-1} and a range of 42 to 223 N h^{-1} yr^{-1} (Fischer et al., 2018). In the Czech Republic, an average R-factor of 64 N h^{-1} yr^{-1} with a range of 32 to 152 N h^{-1} yr^{-1} was found (Hanel et al., 2016). A range of 35 to 138 N h^{-1} yr^{-1} with a mean of 74 N h^{-1} yr^{-1} was observed for 95 Slovakian locations (Onderka and Pecho, 2019).

Using the calculated R-factor and the measured rainfall for each station, a linear relationship of the mean annual R-factor as a function of mean annual rainfall could be established for the VP and A stations, respectively (Fig. 3 and Eq. (6) and (7)).

For the R_{VP} stations, the linear regression (Eq. (6)) produced an R^2 of 0.71, and for the R_A stations, the linear regression (Eq. (7)) produced an R^2 of 0.78.

$$R_{VP} = -26.518 + 0.205P_{VP} \quad (6)$$

$$R_A = -37.358 + 0.179P_A \quad (7)$$

The 95% confidence interval for the slope coefficient for R_{VP} was ±0.020, while it was ±0.019 for R_A. The mean prediction interval was ±59 N h^{-1} yr^{-1} for R_{VP} and ±65 N h^{-1} yr^{-1} for R_A.

3.2. Mapping of rainfall erosivity

To extrapolate the spatial distribution of both R_{VP} and R_A (Fig. 4 and Fig. 5) to the Austrian territory, equations (6) and (7) were applied with the mean VP or A rainfall in each of the SPARTACUS grid cells. The mean prediction intervals of the regressions were used to define the interval of the map classes at 60 N h^{-1} yr^{-1}.

Combining the R_{VP} linear regression with the mean P_{VP} of each SPARTACUS rainfall grid produced an R-factor mean of 133 N h^{-1} yr^{-1} and a range of 49 to 306 N h^{-1} yr^{-1}, with lower R-factor values found in the Northeast (NFH, WMV) and the Southeast (SFH) (Table 3). The highest R-factor values were found in the alpine regions of HA and VA, particularly in the far west, and in the far south of the HA and AOR zones (Fig. 4). These results also coincided with the location of the highest R-factors found in the VP and A stations used for the study, such as stations Bödele, Naßfeld, Ebnit and Zell-Pfarre, which exhibited both the highest R_{VP}- and R_A-factors (see Table A1).

Clear differences in R-factors can be seen between MAPZ. The distribution of R-factors across Austria coincides well with the classification of the MAPZ. This suggests that the division into MAPZ, which was based on soil characteristics, climate, terrain, agricultural production and land use (Wagner, 1990a, 1990b), is also useful considering rainfall erosivity.

Extension of R_A-factors with the P_A data from the SPARTACUS dataset resulted in a mean R-factor of 109 N h^{-1} yr^{-1} and an R-factor range of −16 to 290 N h^{-1} yr^{-1}. Grid cells with a mean annual rainfall of less than 192 mm would result in a negative R-factor based on the R_A regression. The stations used to create the R_A linear regression only reached 1917 m above sea level (Station Kühtai, R_{VP} = 91 N h^{-1} yr^{-1}, R_A = 90 N h^{-1} yr^{-1}), and the extension of our procedure above this altitude may not be representative of the actual erosivity in high alpine environments. Areas experiencing negative R-factors were limited to 58 grid cells of 1 km^2, located exclusively on alpine peaks in the southwestern part of HA, between 2400 and 3800 m above sea level. Similarly, the temperature data grid used in the procedure for temperature correction resulted in the removal of most precipitation data for these areas due to the 0 °C snow threshold. Hiebl and Frei (2016) noted that their data had a discrepancy of up to 1.5 °C in high elevation areas, with a 1.3 °C discrepancy overall. However, the agriculturally important areas are located in the East of Austria, outside the extreme elevations of the Alps. These are the main target areas of the USLE approach, and these areas were unaffected by the precipitation grid temperature correction.

Table 4
Validation statistics for each of the mapped R-factor models compared to rainfall stations. KK: Klik and Konecny (2012), PAN: Panagos et al. (2015a), STR: Strauss et al. (1995), CF: calibration factor.

R-factor models	Validation statistics		
	MAE	RMSE	WI
R_{VP}	23.8	32.5	0.90
R_A	26.5	38.1	0.90
KK R_{VP}	22.7	31.8	0.88
STR R_{VP}	27.6	40.4	0.77
PAN R_{A*CF}	34.7	55.8	0.68
PAN R_A	47.5	69.3	0.67
STR R_A	57.4	77.7	0.54

Our results matched the consensus of erosivity in surrounding countries, albeit some variations existed between R-factors in all surrounding countries. Meusburger et al. (2012) found that the mapped R-factor for Switzerland ranged from 12 to 650 N h^{-1} yr^{-1} with a mean of 122 N h^{-1} yr^{-1}. The authors removed snowfall in the R-factor calculation, which led to lower erosivities in the eastern mountainous part of Switzerland. This corresponds well with the lower R_A-values mapped in the southwestern part of HA in Austria. Based on radar data, Auerswald et al. (2019) found the German R-factor in the southern German mountains along the Austrian border to have values above 185 N h^{-1} yr^{-1}, which corresponds well with our mapped R-factors in northern HA and western VA. On the border to WMV the German R-factor values are higher than our R-factor values. In Slovenia, the range of R-factors was mapped to lie between 102 and 1438 N h^{-1} yr^{-1} (Bezak et al., 2015) with the highest values in the Julian Alps on the border to Austria and Italy and the lowest towards the northeast at the Hungarian and Austrian borders. This coincides with the high R-factors we mapped for southern HA and AOR and the lower R-factors in the East of SFH. The European study by Panagos et al. (2015a) mapped R-factors in Austria between 35 and 435 N h^{-1} yr^{-1} with a mean R-factor of 108 N h^{-1} yr^{-1}. This mean corresponds well with our mean R_A-factor, however the spatial distribution differs.

3.3. Comparison of studies

To look further into the spatial variation in R-factor estimation between studies, we compared the map from Panagos et al. (2015a) and our R_A map. We also mapped the R-factor regressions of Strauss et al. (1995), both annual and summer regressions and Klik and Konecny (2012) on the SPARTACUS rainfall data to compare these regressions to our R-factor maps spatially (Fig. 6).

The range in the difference between the R-factor map of Panagos et al. (2015a) and our annual R-factor map was from −198 N h^{-1} yr^{-1} to 258 N h^{-1} yr^{-1}, with a mean difference of −1.75 N h^{-1} yr^{-1} and a standard deviation of 53.7 N h^{-1} yr^{-1}. Even though the mean difference was only −1.75 N h^{-1} yr^{-1}, the mapping of differences clearly shows significant local discrepancies. In the southern regions of HA, AOR and KB, the differences were high. Here the Panagos et al. (2015a) map

overestimated the R-factors. This is most likely a result of the removal of snowfall from our R-factor calculations. The difference was negative along the border to Germany and in VA, meaning our map has higher R-factors than the Panagos et al. (2015a) map.

The Panagos et al. (2015a) study identified the highest erosivity to radiate northward from the south of Austria while bypassing the high erosivity of the northern Alps. None of the 31 stations used by Panagos et al. (2015a) was located in these areas of Austria, which would highly impact the R-factor mapping. Panagos et al. (2015c) stated that the high R-factors were likely due to interpolation close to Slovenian and Italian stations with very high recorded R-factors. Auerswald et al. (2015) remarked, that the high R-factor values seemed overestimated and was likely due to the inclusion of snowfall in the calculations. By eliminating snowfall from the rainfall data in our study, particularly at high elevation stations with large snowfall amounts, we observed a decrease in R-factors for individual stations compared to the study by Panagos et al. (2015a).

The range in difference between the mapping of the annual Strauss et al. (1995) R-factor equation and our R_A map was from −153 N h^{-1} yr^{-1} to 39 N h^{-1} yr^{-1}, with a mean difference of −39.5 N h^{-1} yr^{-1} and a standard deviation of 25.8 N h^{-1} yr^{-1}. The differences were mainly negative. This suggests that the present study results in higher R-factors compared to the Strauss et al. (1995) equation. The areas with the highest differences were the south of HA and AOR and in VA and along the German border.

Comparing the summer R-factor equation mapping by Strauss et al. (1995) and our R_{VP} map resulted in a range of difference from −105 N h^{-1} yr^{-1} to 6 N h^{-1} yr^{-1}. The mean difference was −30 N h^{-1} yr^{-1} with a standard deviation of 21 N h^{-1} yr^{-1}. Thus, the summer regression of Strauss et al. (1995) performed better with our data compared to the annual regression.

Using the regression of Klik and Konecny (2012) for mapping of R-factors across Austria resulted in the lowest R-factor differences compared to our R_{VP} map. The range in difference was from −36 N h^{-1} yr^{-1} to 9 N h^{-1} yr^{-1} with a mean of −5 N h^{-1} yr^{-1} and a standard deviation of 8.6 N h^{-1} yr^{-1}.

The result of the validation of the mapped R-factors compared to the rainfall station R-factors can be seen in Table 4.

Validation statistics showed that our R_{VP} and R_A maps both agreed well with the rainfall station data. The map using the Klik and Konecny (2012) regression also performed well compared to the rainfall station R-factors. Converting our rainfall station R-factors from 5 min data to 30 min data by applying the calibration factor of 0.7984 (Panagos et al., 2015a) resulted in a slightly better agreement with the map by Panagos et al. (2015a). The R-factors produced with the annual regression by Strauss et al. (1995) generally underestimated R-factors, which resulted in the poorest validation statistics. The comparison clearly shows the importance of testing against observed data and previously derived R-factors for the same study area to illustrate variations and test the sensitivity of the R-factor application (Benavidez et al., 2018). Reasons for the difference in R-factor between the studies could have occurred due to data availability, data period, quality, sample sizes, interpolation method and interpretation (Panagos et al., 2015a). As shown by Hanel et al. (2016), using different KE-I relationships results in a considerable variation in estimated R-factors. In our study, we used the KE-I relationships by van Dijk et al. (2002). The KE-I relationship by Wischmeier and Smith (1978) was used by Strauss et al. (1995), and the KE-I relationship by Brown and Foster (1987) was used by Klik and Konecny (2012) and Panagos et al. (2015a). The Brown and Foster (1987) KE-I

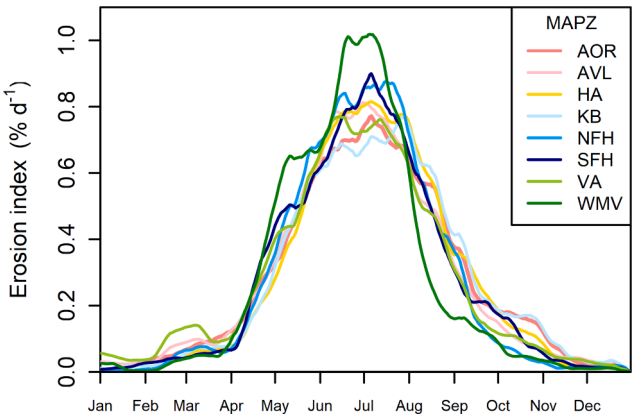

Fig. 7. Daily distribution of the erosion index for each MAPZ in Austria.

relationship used within the RUSLE has previously underestimated KE compared to other relationships. This is evident from the graph of unit rainfall energy vs rainfall intensity (Johannsen et al., 2020; Nearing et al., 2017), and it has thus been recommended to suspend the use of this KE-I relationship (Nearing et al., 2017). Hanel et al. (2016) concluded that the relative importance of the choice of KE-I relationship increases as the number of stations and available years of data increases.

We saw an overall increase in the mean R-factor for Austria for our study. This could have been influenced by the availability of long-term rainfall data with better temporal resolution from a higher number of stations and a wider distribution than previous studies. The majority of stations used in the previous studies were situated in the eastern part of Austria, which receives less rainfall and may have resulted in comparatively lower R-factors. The results by Strauss et al. (1995) were based on analogue rainfall data from 1961 to 1990 from only 15 stations. Topographical variances would not be fully represented, and key erosive events would have been missed. The study by Klik and Konecny (2012) only covered the north-eastern part of Austria and was thus not representative of the whole country. In particular the mountainous part was not included, which would lead to less variability in erosivity. However, the majority of their 51 stations were also included in the present study, contributing to the good agreement with our data and the low MAE and RMSE, although the time series ranged from 9 to 49 years up to 2009 and only from May to October. Our study extended the validity of the erosivity regressions to a larger spatial area thereby increasing the variability. A way to overcome any local variations in R-factors across Austria, would be to make distinct R-factor regression for each MAPZ. Unfortunately, the number of rainfall stations were too low in some regions to do this. The more recent study by Panagos et al. (2015a) obtained data from 1995 to 2010 for the Austrian part of their European erosivity study, but station representation was still poor with only 31 stations used for their spatial regression, albeit expected due to their immense spatial study coverage.

The poorer data resolution used by former studies (15- and 10-minute resolutions) could cause skewed event erosivity based on rainfall duration and intensity. Furthermore, Panagos et al. (2015a) aggregated R-factors of different temporal resolutions to 30 min resolution via a calibration factor for comparability of data from all the European countries, which caused a decrease in R-factors. Despite 5-minute high-resolution data and a significant increase in the number of stations available for this study, station data were not available for all areas of Austria, which affects the calculated erosivity, as identified by Fischer

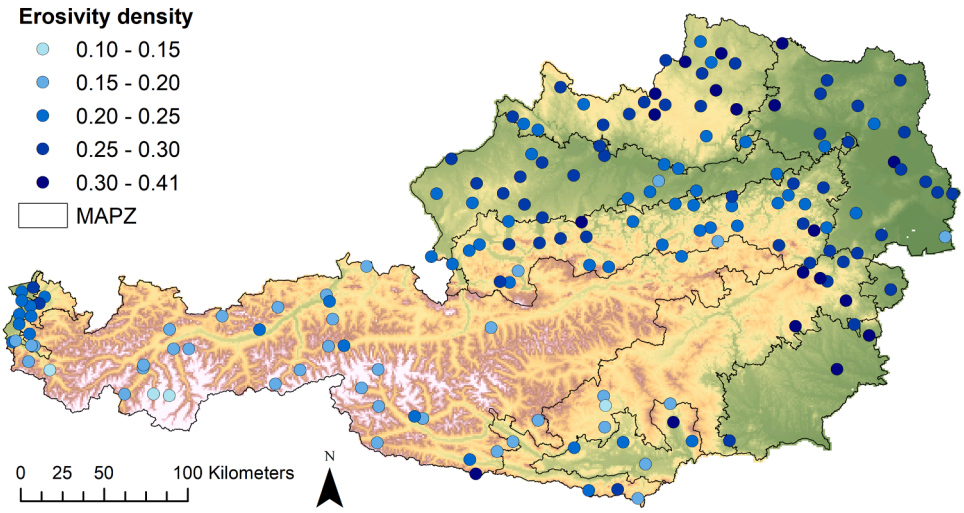

Fig. 8. Regional distribution of erosivity density (N h^{-1} yr^{-1} mm^{-1}) for all rainfall stations across Austria during the vegetation period.

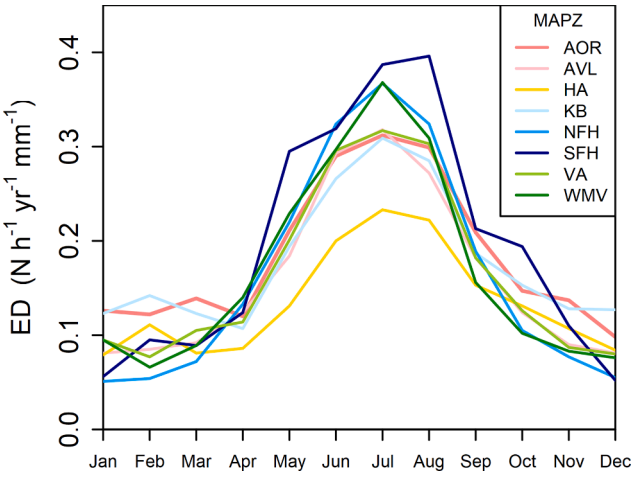

Fig. 9. Mean monthly erosivity density (ED) for all rainfall stations in each MAPZ.

et al. (2018). The availability of rainfall stations with the data needed for event erosivity calculation was also recognised as the main limitation impacting the accuracy of rainfall synchrony scale estimates by Bezak et al. (2021). Radar data has been suggested to improve spatial coverage, although this method also has its drawbacks of lower temporal and spatial resolution than rain gauge data (Fischer et al., 2018). However, improved erosivity estimation based on rain gauge data will be possible for future evaluations with the continuous high-resolution data collection available for Austria.

The type of interpolation or regression analysis will also influence the zonal classification of data (Angulo-Martínez et al., 2009; Hanel et al., 2016). Other studies included covariates such as climatic data, elevation, topography and snow depth in their linear regression to spatially map the R-factor via regression-kriging (Meusburger et al., 2012; Schmidt et al., 2016) or the non-linear approach of Gaussian Process Regression (Panagos et al., 2015a). However, inappropriately chosen covariates may also distort the R-factor estimations (Brychta and Janeček, 2017). We did not interpolate our found at-site R-factors directly, but used the R-factor regressions together with the rainfall data from the SPARTACUS grid. This data grid had already been interpolated via kriging with a set of topographic predictors, cross-validated and error-estimated (Hiebl and Frei, 2018). Error estimates were the largest when looking at the 1-day scale and using the grid values as a point estimate. The error estimates were lowered when interpreting grid point values as area mean values instead and when applying the dataset at larger time scales than single days (see Hiebl and Frei (2018) for further details). The dataset that Hiebl and Frei (2018) used for their rainfall calculations consisted of many more stations compared to our dataset. This is of particular importance for a spatially extremely heterogeneous area like Austria. A comparison of the average VP and A rainfall from station data and the corresponding SPARTACUS grid cell situated at the site of the station were performed for all stations. Calculating the root mean squared error fraction (RMSF) and bias as according to Hiebl and Frei (2018) resulted in a RMSF of 1.05 for both VP and A datasets and a bias of 1.03 and 0.98 for the VP and A datasets, respectively. This was within the same range or better than the error estimates found by Hiebl and Frei (2018). Thus, we believe the dataset to be suitable for our purposes of long-term mean annual rainfall erosivity estimation across Austria. We recognise that our methodology may still be updated in the future as more high-resolution data becomes available. It may also be of interest to uniform R-factor calculation methods across Europe to better compare rainfall erosivity and soil erosion risk areas.

Keeping the described methods of the previous studies in mind, our study updated the calculated R-factors for Austria with a more representative number of rainfall stations, leading to a better spatial distribution of R-factor estimation. The data were also gap-filled and corrected, excluded snowfall and were based on an updated time series, increasing the representativeness of the rainfall erosivity estimation for Austria.

3.4. *Distribution of daily rainfall erosivity and erosivity density*

The seasonal distribution of erosivity in Austria defined as the erosion index (Fig. 7) describes a common European trend of peak daily

erosion index recorded during summer months (Auerswald et al., 2019; Ballabio et al., 2017; Meusburger et al., 2012; Schmidt et al., 2016), and the lowest erosion index, falling below 0.1% d^{-1}, being observed during the winter months (October to April). The maximum measured daily erosivity was observed in July for most MAPZs and ranged between 1.02% d^{-1} in WMV and 0.77% d^{-1} in KB. The percentage of erosivity occurring in the months defined as the vegetation period, from April until October, amounted to 94% of the average annual erosivity for all of Austria, of which WMV and NFH tied for the highest VP erosivity percentage at 96%.

The temporal erosivity distribution in WMV stands out from the distribution of the other MAPZs, which otherwise follow quite similar distributions of daily erosivity. The distribution for WMV peaks earlier in May, has the highest peak in July and declines more in August than the other MAPZs. A peak in erosivity in the early stages of the vegetation period could increase the risk of soil erosion as the soil is still bare or sparsely covered by crops. The high variability of erosivity throughout the year clearly demonstrates the need to estimate the temporally distributed R-factor. Furthermore, the temporal distribution of erosivity throughout the year is necessary to calculate the C-factor and enable Austria's soil erosion risk assessment based on RUSLE. The distinction into MAPZs has the benefit of creating a more accurate risk assessment based on climatic variability and thereby an improved adaptation of preventative erosion management in each zone. This is especially important because increasing precipitation and erosivity was already found for rainfall stations in the eastern part of Austria (Klik and Konecny, 2012), and predictions for 2040–2060 suggest a possible increase in highly erosive rain events (Klik and Eitzinger, 2010). Furthermore, other factors influencing future soil erosion rates such as land use patterns and agro-environmental policies (Panagos et al., 2021) can be better managed at the defined local level of each MAPZ.

Areas at risk of soil erosion can be further identified by calculating the erosivity density, which expresses whether high rainfall erosivity results from the accumulation of large rainfall amounts or intense events with lower rainfall amounts. The influence of rainfall intensity on erosivity enables the identification of regional and seasonal variability in soil erosion susceptibility. All stations measuring during the vegetation period were used to calculate the spatial distribution of erosivity density in Austria (Fig. 8).

The spatial distribution of mean erosivity density across the MAPZs during the vegetation period produced a national average of 0.24 N h^{-1} yr^{-1} mm^{-1}, ranging from 0.10 N h^{-1} yr^{-1} mm^{-1} in HA to 0.41 N h^{-1} yr^{-1} mm^{-1} in AOR (Fig. 8). The zone with the highest mean erosivity density was SFH, and the lowest mean ED was found in HA (Table 2). However, when comparing erosivity density to the R-factor maps, the highest erosivity density coincided with areas of low R-factors along the northern and eastern Austrian border. Despite NFH and WMV having the two lowest mean R-factors, these two MAPZs had the highest erosivity densities after SFH. This demonstrates that these areas are more affected by high-intensity erosive rainfalls, which pose a real risk in these areas of significant agricultural value.

The yearly variability in erosivity density (Fig. 9) for all rainfall measurement stations within this study (both A and VP stations) showed the highest ED in summer, with July having a mean ED of 0.31 N h^{-1} yr^{-1} mm^{-1}. During the winter months, the mean ED fell below 0.1 N h^{-1} yr^{-1} mm^{-1}, which indicates that rainfall erosivity is not driven by rainfall intensity in this period. A similar seasonal variation in ED was found in Switzerland (Schmidt et al., 2016) and East/Central European countries (Panagos et al., 2016).

4. Conclusions

This study updated the R-factor estimation for Austria and generated R-factors for the main agricultural production zones. We employed a significantly larger number of rainfall stations than previous studies, leading to a better spatial distribution of R-factor estimation. To improve the data quality, data were gap-filled and corrected, excluded snowfall and were based on an updated long-term time series, increasing the representativeness of the rainfall erosivity estimation for Austria.

Based on the rainfall station data, two linear regressions describing the R-factor as a function of mean rainfall amount were established for the vegetation period (Apr-Oct) and annually. Extending the point source data to a rainfall erosivity map with full spatial coverage for Austria was done by applying the regressions to the 1 km^2 daily rainfall grids from the SPARTACUS dataset. A spatial comparison of the R-factor maps with previous studies revealed considerable differences in local R-factor estimation between studies. Thus, an updated and spatially well-distributed erosivity map is essential for precise soil erosion risk assessment. Areas at risk of soil erosion and the timing of vulnerability could be observed from differences in the temporal and spatial distribution of rainfall erosivity, erosivity index and erosivity density between the main agricultural production zones. The highest erosivity (densities) were found in the agriculturally important eastern regions of Austria during the summer months. This serves as a basis for updating the Austrian soil erosion risk map at the spatial scale of agricultural parcels for improved soil management and mitigation implementation during times of high impact rainfall.

Despite the use of high-resolution data, extreme erosive events can influence the mean annual R-factor and may need to be accounted for depending on their probability of occurrence. Based on future predictions of increased erosive rainfall events and R-factor, future studies should focus on the trends and changes in annual erosive rainfall and R-factor for Austria over an extended period of long-term rain gauge data.

Declaration of Competing Interest

The authors declare that they have no known competing financial interests or personal relationships that could have appeared to influence the work reported in this paper.

Acknowledgements

This work has partially been funded within the projects ACRP13 - EROS-A - KR20AC0K17974, of the Klima- und Energiefonds Österreich and EROS-AT, of the Austrian Ministry for Agriculture, Regions and Tourism.

Appendix A

See Table A1.

Table A1
All rainfall station data before (BC) and after data correction including mean rainfall amount (P_{VP}) and rainfall erosivity (R_{VP}) during the vegetation period and mean annual rainfall (P_A) and annual rainfall erosivity (R_A).

Station	Longitude	Latitude	Elevation (m)	Runtime (years)	P_{VP}_BC	P_{VP}	R_{VP}_BC	R_{VP}	P_A_BC	P_A	R_A_BC	R_A
Alberschwende	9.849166667	47.45833333	717	21	1275	1276	244	246				
Alland (Autobahnmeisterei)	16.06638889	48.06777778	339	21	512	513	80	92	693	702	86	99
Almsee-Fischerau	13.95083333	47.82388889	574	21	1074	1077	215	230				
Altach	9.654722222	47.35916667	412	21	878	881	134	138	967	976	138	163
Altmanns	15.10666667	48.87138889	590	21	523	532	64	67				
Amerlügen (Saminaweg)	9.612222222	47.20833333	760	21	912	913	134	137				
Andau	17.02527778	47.77555556	119	21	377	378	35	37				
Annaberg	15.36805556	47.87583333	924	21	1006	1013	151	153				
Attersee	13.53638889	47.91833333	495	21	777	779	130	133				
Ausseraigen	16.07222222	47.56222222	681	21	706	710	132	135				
Bad Goisern	13.61305556	47.65166667	505	21	1014	1015	147	152	1453	1455	173	181
Bärental	14.15583333	46.46888889	1000	19	872	985	165	222	1202	1647	205	279
Behamberg	14.49583333	48.03555556	495	21	723	725	110	114	943	945	118	121
Bleistätter Moor	14.04638889	46.69833333	510	21	524	554	81	109	688	797	92	122
Blumau	16.32138889	47.92361111	233	21	426	428	58	60				
Bödele	9.808611111	47.42111111	1150	21	1608	1610	381	389	1946	1954	406	414
Brand	9.745555556	47.10777778	1005	21	1013	1013	134	135				
Brandl-Koralpe	14.96944444	46.72472222	1485	19	651	721	106	139	708	891	107	142
Braunau am Inn	13.07666667	48.25388889	360	21	585	587	90	94				
Bregenz (Altreuteweg)	9.756666667	47.50722222	447	21	1121	1126	250	253	1554	1562	274	277
Breitenfeld	15.38638889	48.74833333	568	21	482	486	75	80	594	601	78	83
Bromberg	16.205	47.66333333	419	21	643	648	112	113	774	799	117	119
Deutsch Jahrndorf	17.10111111	48.00361111	131	21	383	384	58	61				
Deutsch Kaltenbrunn	16.12416667	47.08944444	358	21	492	500	96	107	624	633	102	113
Dornbirn	9.738611111	47.40472222	441	21	1067	1067	191	197				
Dreifaltigkeit	14.28666667	46.80666667	1180	21	568	598	64	83	669	659	70	91
Durlaßboden	12.10944444	47.23972222	1432	21	881	891	107	113	958	975	107	113
Dürnbach im Burgenland	16.38861111	47.26305556	292	21	467	473	96	106	586	594	100	110
Ebensee (Wasserwerk)	13.78388889	47.80055556	422	21	1036	1044	210	217				
Ebenwald	15.69833333	47.99138889	1034	21	797	826	121	146				
Ebnit	9.749444444	47.35111111	1051	21	1473	1478	302	313	1852	1860	327	338
Felbertauerntunnel-Süd	12.50555556	47.11833333	1637	21	988	989	109	109	1059	1061	113	114
Flachau	13.39583333	47.34722222	910	21	788	799	101	106	946	972	105	111
Flachberg	16.08861111	48.28833333	179	21	561	568	88	92				
Frankenburg	13.49333333	48.06777778	515	21	692	696	127	130				
Frankenfels	15.32777778	47.9825	468	21	927	935	163	172	1364	1394	199	209
Franzensdorf	16.64333333	48.19	152	21	418	420	72	74	547	550	74	77
Frastanz	9.635833333	47.21666667	487	21	884	887	124	126	1176	1179	135	136
Friedburg	13.2475	48.01722222	512	21	751	755	131	157				
Furth-Harras	15.915	47.98138889	488	21	680	683	112	114				
Fuschl	13.30472222	47.79333333	670	21	748	791	118	159				
Fussach	9.665	47.48166667	400	21	907	912	154	159				
Gänserndorf	16.73638889	48.34694444	151	21	387	392	53	56	483	490	55	59
Gattendorf	16.98194444	48.01583333	150	21	390	390	57	71				
Geboltskirchen	13.63277778	48.15722222	540	21	670	678	116	126				
Gepatsch-Damm	10.73888889	46.96083333	1651	21	586	587	41	43	651	657	42	44
Ginzersdorf	16.72055556	48.62777778	176	21	393	394	60	60	502	505	62	62
Glaserbrücke-Farchtensee	13.44194444	46.68138889	990	19	578	626	82	97				
Gloggnitz	15.93944444	47.66416667	509	21	578	586	107	109	711	726	111	113
Gmünd	14.97972222	48.76416667	498	20	486	488	88	97	604	608	91	99
Gmunden-Traundorf	13.80694444	47.93666667	456	21	792	799	139	145				
Gosau	13.54194444	47.58972222	765	21	1136	1141	198	203	1489	1499	215	221
Grades-Klachl	14.28083333	46.975	725	21	557	574	71	84	671	730	77	92
Gresten	15.0225	47.99222222	398	21	786	793	121	124	1130	1147	143	146
Grieskirchen-Moosham	13.80916667	48.23277778	352	21	533	534	80	82				
Großgmain	12.91916667	47.72805556	560	21	843	847	122	123				
Gutenstein	15.89444444	47.8775	478	21	669	672	127	130				
Hainfeld	15.78416667	48.03305556	429	21	649	649	89	91	817	822	97	98
Hallein	13.08861111	47.68805556	443	21	811	816	113	115	1143	1169	131	134
Helfenberg	14.14777778	48.545	598	21	539	547	71	83	594	615	73	110
Hellmonsödt	14.30416667	48.43305556	840	21	628	633	109	114				
Hintersee	13.2225	47.76111111	727	21	851	957	138	213				
Hochegg	13.56638889	46.73333333	1030	19	555	607	66	82	711	795	76	93
Hochkar (Sportheim)	14.9175	47.71833333	1500	19	1028	1034	178	191				
Hochneukirchen	16.215	47.455	736	21	631	636	128	129				
Hohe Wand (Herrgottschn. haus)	16.08055556	47.85194444	828	21	519	525	84	90				
Hollabrunn	16.07138889	48.57166667	236	21	435	436	69	72	551	553	71	73
Hollenstein an der Ybbs	14.76527778	47.78333333	495	21	1045	1053	182	185	1439	1451	209	213
Hollern	16.89055556	48.07583333	145	21	428	433	70	71	588	597	74	75
Hopfgarten i.Def.	12.51277778	46.91972222	1096	21	692	694	78	79	826	833	87	88
Huttererböden	14.18055556	47.67972222	1370	21	755	764	106	125	900	934	109	130

(*continued on next page*)

Table A1 (*continued*)

Station	Longitude	Latitude	Elevation (m)	Runtime (years)	P_{VP}_BC	P_{VP}	R_{VP}_BC	R_{VP}	P_A_BC	P_A	R_A_BC	R_A
Ibm	12.95944444	48.06694444	427	21	687	693	110	117				
Immendorf	16.12861111	48.6425	237	21	396	410	69	71	499	543	71	72
Innerlaterns	9.743055556	47.25694444	1025	21	1229	1237	198	204				
Iselsberg-Penzelberg	12.85861111	46.85666667	1210	19	614	632	66	76	742	813	74	87
Karlstift	14.72944444	48.59583333	919	21	686	697	126	133	770	794	128	135
Kartitsch	12.50222222	46.725	1374	21	760	775	104	109	911	963	116	124
Kelchsau	12.13888889	47.38638889	801	21	1005	1007	129	130	1205	1208	136	138
Kierling	16.28166667	48.3075	232	21	482	488	69	79	655	678	74	82
Kirchbichl	12.0875	47.51666667	496	21	706	723	96	113	924	972	102	121
Kirchdorf an der Krems	14.12111111	47.91138889	456	21	776	780	155	161				
Klaus an der Pyhrnbahn	14.15888889	47.83166667	461	21	918	927	184	203				
Klopein am Klopeiner See	14.60166667	46.60555556	470	20	596	609	81	95	767	824	90	105
Kopfing	13.66027778	48.44138889	569	21	636	638	95	101				
Kössen	12.40277778	47.67166667	590	21	1053	1054	147	149	1450	1451	170	173
Kühtai	11.00638889	47.20777778	1917	21	850	861	87	91	859	886	86	90
Lackenhof	15.15388889	47.87	807	19	1180	1192	214	219	1501	1513	237	246
Ladis-Neuegg	10.64888889	47.09722222	1426	21	634	636	59	60	692	700	60	61
Lasberg	14.51527778	48.48833333	575	21	515	517	78	81				
Lichtenau	15.38666667	48.50194444	666	21	496	497	84	85	603	604	86	87
Liebenau	14.80916667	48.53444444	953	21	597	602	98	105				
Limbach	15.11305556	48.7	575	21	500	502	75	79	659	664	79	83
Linz (Wasserwerk Scharlinz)	14.31166667	48.26666667	260	21	556	560	79	83	764	773	85	90
Linz-Urfahr	14.27527778	48.32	305	19	535	535	80	85				
Ludesch	9.784722222	47.19277778	550	21	818	870	89	104				
Lunz am See	15.06861111	47.855	611	21	1052	1059	162	168	1444	1457	187	194
Lustenau	9.668888889	47.43361111	404	20	841	843	144	148	1137	1151	155	159
Magdalensberg	14.43055556	46.725	920	21	565	598	83	109	689	794	91	116
Maria Langegg	15.45416667	48.32527778	495	21	499	502	70	72				
Miesenbach	15.98194444	47.83777778	480	21	619	632	122	125	858	897	132	137
Münzkirchen	13.57111111	48.47972222	498	21	601	605	97	106				
Naglern	16.37	48.49972222	280	21	438	440	64	66	551	528	67	69
Nassereith	10.84972222	47.31055556	854	21	672	673	65	65	868	869	72	72
Naßfeld	13.27583333	46.56027778	1530	21	893	1090	231	350	1114	1745	254	382
Naßwald	15.69666667	47.76444444	619	21	891	897	172	176	1185	1199	188	192
Nebersdorf	16.57333333	47.505	225	21	438	442	81	91	562	579	84	95
Neuhaus am Zellerain	15.20861111	47.79555556	1076	18	991	998	135	133	1236	1244	148	147
Neukirchen am Walde	13.77583333	48.40833333	555	21	588	589	77	82				
Neumarkt im Hausruck	13.72472222	48.27805556	398	21	566	568	80	84				
Neunkirchen	16.09888889	47.72666667	361	21	498	508	91	94	611	629	94	97
Neustadtl	14.90583333	48.19111111	486	21	701	702	106	108				
Neustift an der Rosalia	16.31861111	47.70722222	597	21	603	606	119	122				
Oed	14.74583333	48.12638889	401	21	542	542	58	60				
Oetz	10.88611111	47.20583333	760	21	568	574	56	60	702	713	60	64
Orth an der Donau	16.69666667	48.14888889	149	21	411	415	63	71	536	542	66	74
Pechgraben	14.53305556	47.91027778	430	21	849	852	139	161	1250	1257	165	191
Penzelberg-Iselsberg	12.85944444	46.85777778	1210	21	658	670	70	80	801	850	79	92
Pertisau	11.70333333	47.44388889	930	21	1033	1046	142	150	1286	1327	155	165
Pfunds	10.51111111	46.95277778	992	21	534	534	60	65	718	720	65	70
Poggschlag	15.13722222	48.36222222	904	21	551	555	71	75				
Pöllau (Zentralstation)	15.80861111	47.32666667	525	21	665	681	181	195	799	826	187	203
Prägraten	12.37555556	47.01805556	1340	21	679	684	67	69	792	805	74	75
Preblau	14.80388889	46.92805556	790	20	605	625	82	96	712	793	89	102
Pyhra	15.69666667	48.14861111	298	21	642	650	98	99	829	841	104	106
Pyhrabruck	14.82083333	48.77388889	539	21	539	545	80	85				
Rappottenstein	15.09611111	48.52444444	586	21	531	535	79	83				
Riegersburg	15.77305556	48.84972222	451	21	452	457	76	78	554	563	78	80
Runserau	10.6525	47.11444444	859	21	595	596	60	60	744	746	63	64
Rußbach am Paß Gschütt	13.46638889	47.59388889	810	21	958	992	172	182	1220	1249	194	199
Sandl	14.63944444	48.55083333	935	21	651	656	106	115				
Saxen-Au	14.79111111	48.21472222	244	21	481	483	63	74				
Scharnitz	11.26388889	47.38944444	959	21	898	902	102	103	1071	1075	107	109
Schlägl	13.96111111	48.63805556	555	21	559	560	89	92				
Schlegeis	11.69583333	47.03138889	1800	21	871	873	91	95	898	909	93	96
Schönberg	15.69666667	48.5175	217	21	407	410	61	64	511	516	63	66
Seeberg	14.53805556	46.42194444	1040	21	915	954	133	151	1216	1392	159	185
Spital am Pyhrn	14.33472222	47.66888889	630	21	959	965	136	141	1327	1338	156	160
St.Corona am Wechsel	16.01666667	47.58083333	870	21	776	785	191	193	901	913	198	201
St.Johann am Walde	13.28	48.1225	629	19	791	800	136	146	1051	1085	147	160
St.Leonhard am Walde	14.87444444	48.00194444	634	21	819	819	124	138				
St.Martin i.G.	11.56166667	47.32166667	875	21	926	929	151	155				
St.Oswald	13.76555556	46.84777778	1373	19	682	756	93	105	806	911	102	116
Stadtschlaining	16.27388889	47.32611111	424	21	407	414	86	128				
Steinakirchen am Forst	15.04555556	48.06972222	338	21	575	581	77	112				
Stillupp	11.88888889	47.10972222	1125	21	847	851	103	109	978	989	110	117
Stollberg	15.82666667	48.09444444	583	21	633	636	107	119				

(*continued on next page*)

Table A1 (*continued*)

Station	Longitude	Latitude	Elevation (m)	Runtime (years)	P_{VP_BC}	P_{VP}	R_{VP_BC}	R_{VP}	P_{A_BC}	P_A	R_{A_BC}	R_A
Texing	15.33222222	48.03388889	469	21	736	739	126	132				
Thüringen	9.762777778	47.19527778	547	21	939	940	108	110	1274	1275	122	123
Trattenbach (Schlaggraben)	15.88194444	47.615	1100	21	778	788	182	185	864	879	187	190
Tschagguns	9.915833333	47.0675	681	21	843	851	90	91	1158	1173	101	102
Tulln-Bildeiche	16.05472222	48.35722222	177	21	442	444	61	67				
Ulrichskirchen	16.49472222	48.39888889	183	21	418	418	54	56	559	560	58	59
Vitis	15.19	48.75722222	526	21	484	486	62	65				
Vöcklabruck	13.66555556	48.00777778	423	21	684	687	124	136				
Waidegg	13.22916667	46.6375	635	20	815	881	146	178	1156	1429	179	226
Waidhofen an der Thaya	15.27416667	48.805	498	21	456	459	76	77	578	583	78	79
Wald	12.23333333	47.24388889	860	21	744	744	97	98	917	918	115	116
Weiler	9.656111111	47.30638889	500	21	945	948	155	158				
Weißenbach am Attersee	13.53916667	47.79472222	476	21	1047	1056	214	214				
Weitersfelden-Ritzenedt	14.72277778	48.48416667	764	21	591	594	102	127				
Wels	14.06277778	48.16222222	305	21	566	571	86	92				
Wf-Taschachbach	10.86277778	46.95472222	1798	21	502	502	25	25	543	546	25	26
Wies	15.26194444	46.7225	390	21	740	745	151	162				
Winklern ob Straßburg	14.29416667	46.92305556	1040	19	428	502	59	66	521	596	65	71
Wolfsbach	14.67305556	48.06916667	343	21	603	605	81	84	815	820	87	90
Wolfsberg	14.82638889	46.82777778	440	19	568	606	111	128	696	727	118	135
Wörgl	12.11138889	47.48138889	605	21	793	798	107	134	999	1009	113	141
Wulkaprodersdorf	16.51805556	47.80055556	164	21	401	410	57	67	525	550	61	70
Zell-Pfarre	14.38111111	46.47222222	900	20	872	1042	193	257	1124	1752	228	319
Zettersfeld	12.79416667	46.8675	1903	21	766	771	115	145				
Zwettl-Edelhof	15.22444444	48.60666667	595	21	527	531	91	92	631	637	93	94

References

Angulo-Martínez, M., López-Vicente, M., Vicente-Serrano, S.M., Beguería, S., 2009. Mapping rainfall erosivity at a regional scale: a comparison of interpolation methods in the Ebro Basin (NE Spain). Hydrol. Earth Syst. Sci. 13, 1907–1920.

Auerswald, K., Fiener, P., Gomez, J.A., Govers, G., Quinton, J.N., Strauss, P., 2015. Comment on "Rainfall erosivity in Europe" by Panagos et al. (Sci. Total Environ., 511, 801–814, 2015). Sci. Total Environ. 532, 849–852.

Auerswald, K., Fischer, F.K., Winterrath, T., Brandhuber, R., 2019. Rain erosivity map for Germany derived from contiguous radar rain data. Hydrol. Earth Syst. Sci. 23, 1819–1832. https://doi.org/10.5194/hess-23-1819-2019.

Ballabio, C., Borrelli, P., Spinoni, J., Meusburger, K., Michaelides, S., Beguería, S., Klik, A., Petan, S., Janeček, M., Olsen, P., Aalto, J., Lakatos, M., Rymszewicz, A., Dumitrescu, A., Tadić, M.P., Diodato, N., Kostalova, J., Rousseva, S., Banasik, K., Alewell, C., Panagos, P., 2017. Mapping monthly rainfall erosivity in Europe. Sci. Total Environ. 579, 1298–1315. https://doi.org/10.1016/j.scitotenv.2016.11.123.

Benavidez, R., Jackson, B., Maxwell, D., Norton, K., 2018. A review of the (Revised) Universal Soil Loss Equation ((R)USLE): with a view to increasing its global applicability and improving soil loss estimates. Hydrol. Earth Syst. Sci. 22, 6059–6086. https://doi.org/10.5194/hess-22-6059-2018.

Bezak, N., Ballabio, C., Mikoš, M., Petan, S., Borrelli, P., Panagos, P., 2020. Reconstruction of past rainfall erosivity and trend detection based on the REDES database and reanalysis rainfall. J. Hydrol. 590, 125372 https://doi.org/10.1016/j.jhydrol.2020.125372.

Bezak, N., Borrelli, P., Panagos, P., 2021. A first assessment of rainfall erosivity synchrony scale at pan-European scale. CATENA 198, 105060. https://doi.org/10.1016/j.catena.2020.105060.

Bezak, N., Rusjan, S., Petan, S., Sodnik, J., Mikoš, M., 2015. Estimation of soil loss by the WATEM/SEDEM model using an automatic parameter estimation procedure. Environmental Earth Sciences 74, 5245–5261. https://doi.org/10.1007/s12665-015-4534-0.

Boardman, J., Poesen, J. (Eds.), 2006. Soil Erosion in Europe. John Wiley & Sons, Ltd, Chichester, UK.

Brown, L.C., Foster, G.R., 1987. Storm erosivity using idealized intensity distributions. Transactions of the ASAE 30, 379–386.

Brychta, J., Janeček, M., 2017. Evaluation of discrepancies in spatial distribution of rainfall erosivity in the Czech Republic caused by different approaches using GIS and geostatistical tools. Soil and Water Research 12, 117–127. https://doi.org/10.17221/176/2015-SWR.

Burt, T., Boardman, J., Foster, I., Howden, N., 2016. More rain, less soil: long-term changes in rainfall intensity with climate change. Earth Surf. Proc. Land. 41, 563–566. https://doi.org/10.1002/esp.3868.

Diodato, N., Borrelli, P., Fiener, P., Bellocchi, G., Romano, N., 2017. Discovering historical rainfall erosivity with a parsimonious approach: A case study in Western Germany. J. Hydrol. 544, 1–9. https://doi.org/10.1016/j.jhydrol.2016.11.023.

Fiener, P., Neuhaus, P., Botschek, J., 2013. Long-term trends in rainfall erosivity–analysis of high resolution precipitation time series (1937–2007) from Western Germany. Agric. For. Meteorol. 171–172, 115–123. https://doi.org/10.1016/j.agrformet.2012.11.011.

Fischer, F.K., Winterrath, T., Auerswald, K., 2018. Temporal- and spatial-scale and positional effects on rain erosivity derived from point-scale and contiguous rain data. Hydrol. Earth Syst. Sci. 22, 6505–6518. https://doi.org/10.5194/hess-22-6505-2018.

Hanel, M., Máca, P., Bašta, P., Vlnas, R., Pech, P., 2016. The rainfall erosivity factor in the Czech Republic and its uncertainty. Hydrol. Earth Syst. Sci. 20, 4307–4322. https://doi.org/10.5194/hess-20-4307-2016.

Hiebl, J., Frei, C., 2018. Daily precipitation grids for Austria since 1961—development and evaluation of a spatial dataset for hydroclimatic monitoring and modelling. Theor. Appl. Climatol. 132, 327–345. https://doi.org/10.1007/s00704-017-2093-x.

Hiebl, J., Frei, C., 2016. Daily temperature grids for Austria since 1961—concept, creation and applicability. Theor. Appl. Climatol. 124, 161–178. https://doi.org/10.1007/s00704-015-1411-4.

Horrigan, L., Lawrence, R.S., Walker, P., 2002. How sustainable agriculture can address the environmental and human health harms of industrial agriculture. Environ. Health Perspect. 110 (5), 445–456.

Johannsen, L.L., Zambon, N., Strauss, P., Dostal, T., Neumann, M., Zumr, D., Cochrane, T.A., Klik, A., 2020. Impact of Disdrometer Types on Rainfall Erosivity Estimation. Water 12, 963. https://doi.org/10.3390/w12040963.

Kinnell, P.I.A., 2010. Event soil loss, runoff and the Universal Soil Loss Equation family of models: A review. J. Hydrol. 385, 384–397. https://doi.org/10.1016/j.jhydrol.2010.01.024.

Klik, A., Eitzinger, J., 2010. Impact of climate change on soil erosion and the efficiency of soil conservation practices in Austria. The Journal of Agricultural Science 148, 529–541. https://doi.org/10.1017/S0021859610000158.

Klik, A., Konecny, F., 2012. Rainfall Erosivity in Northeastern Austria. Trans. ASABE 56, 719–725. https://doi.org/10.13031/2013.42677.

Leek, R., Olsen, P., 2006. Modelling climatic erosivity as a factor for soil erosion in Denmark: changes and temporal trends. Soil Use Manag. 16, 61–65. https://doi.org/10.1111/j.1475-2743.2000.tb00175.x.

Lukić, T., Lukić, A., Basarin, B., Ponjiger, T.M., Blagojević, D., Mesaroš, M., Milanović, M., Gavrilov, M., Pavić, D., Zorn, M., Komac, B., Miljković, Đ., Sakulski, D., Babić-Kekez, S., Morar, C., Janićević, S., 2019. Rainfall erosivity and extreme precipitation in the Pannonian basin. Open Geosciences 11, 664–681. https://doi.org/10.1515/geo-2019-0053.

Meusburger, K., Steel, A., Panagos, P., Montanarella, L., Alewell, C., 2012. Spatial and temporal variability of rainfall erosivity factor for Switzerland. Hydrol. Earth Syst. Sci. 16, 167–177. https://doi.org/10.5194/hess-16-167-2012.

Nearing, M.A., Yin, S.-Q., Borrelli, P., Polyakov, V.O., 2017. Rainfall erosivity: An historical review. Catena 157, 357–362.

Onderka, M., Pecho, J., 2019. Update of the erosive rain factor in Slovakia using data from the period 1961–2009. Contributions to Geophysics and Geodesy 49, 355–371. https://doi.org/10.2478/congeo-2019-0018.

Panagos, P., Ballabio, C., Borrelli, P., Meusburger, K., Klik, A., Rousseva, S., Tadić, M.P., Michaelides, S., Hrabalíková, M., Olsen, P., Aalto, J., Lakatos, M., Rymszewicz, A., Dumitrescu, A., Beguería, S., Alewell, C., 2015a. Rainfall erosivity in Europe. Sci. Total Environ. 511, 801–814. https://doi.org/10.1016/j.scitotenv.2015.01.008.

Panagos, P., Ballabio, C., Himics, M., Scarpa, S., Matthews, F., Bogonos, M., Poesen, J., Borrelli, P., 2021. Projections of soil loss by water erosion in Europe by 2050. Environ. Sci. Policy 124, 380–392. https://doi.org/10.1016/j.envsci.2021.07.012.

Panagos, P., Ballabio, C., Meusburger, K., Spinoni, J., Alewell, C., Borrelli, P., 2017. Towards estimates of future rainfall erosivity in Europe based on REDES and WorldClim datasets. J. Hydrol. 548, 251–262. https://doi.org/10.1016/j.jhydrol.2017.03.006.

Panagos, P., Borrelli, P., Poesen, J., Ballabio, C., Lugato, E., Meusburger, K., Montanarella, L., Alewell, C., 2015b. The new assessment of soil loss by water erosion in Europe. Environ. Sci. Policy 54, 438–447. https://doi.org/10.1016/j.envsci.2015.08.012.

Panagos, P., Borrelli, P., Spinoni, J., Ballabio, C., Meusburger, K., Beguería, S., Klik, A., Michaelides, S., Petan, S., Hrabalíková, M., Olsen, P., Aalto, J., Lakatos, M., Rymszewicz, A., Dumitrescu, A., Perčec Tadić, M., Diodato, N., Kostalova, J., Rousseva, S., Banasik, K., Alewell, C., 2016. Monthly rainfall erosivity: Conversion factors for different time resolutions and regional assessments. Water (Switzerland) 8 (4), 119.

Panagos, P., Meusburger, K., Ballabio, C., Borrelli, P., Beguería, S., Klik, A., Rymszewicz, A., Michaelides, S., Olsen, P., Tadić, M.P., Aalto, J., Lakatos, M., Dumitrescu, A., Rousseva, S., Montanarella, L., Alewell, C., 2015c. Reply to the comment on "Rainfall erosivity in Europe" by Auerswald et al. Science of The Total Environment 532, 853–857. https://doi.org/10.1016/j.scitotenv.2015.05.020.

Petek, M., Mikoš, M., Bezak, N., 2018. Rainfall erosivity in Slovenia: Sensitivity estimation and trend detection. Environ. Res. 167, 528–535. https://doi.org/10.1016/j.envres.2018.08.020.

Renard, K.G., Foster, G.R., Weesies, G.A., McCool, D.K., Yoder, D.C., 1997. Predicting Soil Erosion by Water: A Guide to Conservation Planning With the Revised Universal Soil Loss Equation (RUSLE). USA, U.S, Department of Agriculture, Washington, DC.

Sanchez-Moreno, J.F., Mannaerts, C.M., Jetten, V., 2014. Rainfall erosivity mapping for Santiago Island, Cape Verde. Geoderma 217–218, 74–82. https://doi.org/10.1016/j.geoderma.2013.10.026.

Schmidt, S., Alewell, C., Panagos, P., Meusburger, K., 2016. Regionalization of monthly rainfall erosivity patterns in Switzerland. Hydrol. Earth Syst. Sci. 20, 4359–4373. https://doi.org/10.5194/hess-20-4359-2016.

Schwertmann, U., Vogl, W., Kainz, M., 1987. Bodenerosion durch Wasser: Vorhersage des Abtrags und Bewertung von Gegenmaßnahmen. Ulmer, Stuttgart.

Strauss, P., Auerswald, K., Klaghofer, E., Blum, W.E.H., 1995. Rainfall Erosivity: A Comparison Austria-Bavaria. Zeitschrift für Kulturtechnik und Landentwicklung 36, 304–308.

USDA-ARS, 2013. Science Documentation Revised Universal Soil Loss Equation Version 2. Washington D.C.

van Dijk, A.I.J.M., Bruijnzeel, L.A., Rosewell, C.J., 2002. Rainfall intensity-kinetic energy relationships: A critical literature appraisal. J. Hydrol. 261, 1–23. https://doi.org/10.1016/S0022-1694(02)00020-3.

Verstraeten, G., Poesen, J., Demarée, G., Salles, C., 2006. Long-term (105 years) variability in rain erosivity as derived from 10-min rainfall depth data for Ukkel (Brussels, Belgium): Implications for assessing soil erosion rates. Journal of Geophysical Research Atmospheres 111. https://doi.org/10.1029/2006JD007169.

Wagner, K., 1990a. Neuabgrenzung landwirtschaftlicher Produktionsgebiete in Österreich. Teil I (Burgenland, Niederösterreich, Wien, Steiermark, Kärnten). Bundesanstalt für Agrarwirtschaft, Wien.

Wagner, K., 1990b. Neuabgrenzung landwirtschaftlicher Produktionsgebiete in Österreich. Teil II (Oberösterreich, Salzburg, Tirol, Vorarlberg). Bundesanstalt für Agrarwirtschaft, Wien.

Wischmeier, W.H., Smith, D.D., 1978. Predicting rainfall erosion losses - A guide to conservation planning. U.S. Department of Agriculture, Washington, DC, USA.

Xie, Y., Yin, S.-Q., Liu, B.-Y., Nearing, M.A., Zhao, Y., 2016. Models for estimating daily rainfall erosivity in China. J. Hydrol. 535, 547–558.